
Article:
Herrnsdorf, Johannes, Wang, Yue orcid.org/0000-0002-2482-005X, McKendry, Jonathan et al. (9 more authors) (2013) Micro-LED pumped polymer laser:a discussion of future pump sources for organic lasers. Laser & Photonics Reviews. pp. 1065-1078. ISSN: 1863-8899

https://doi.org/10.1002/lpor.201300110

Laser Photonics Rev. **7,** No. 6, 1065–1078 (2013) / **DOI** 10.1002/lpor.201300110

LASER & PHOTONICS REVIEWS

Abstract Optical pumping conditions for organic solid-state lasers (OSLs) are discussed with particular emphasis on the use of gallium nitride based light-emitting diodes (LEDs) as pump sources. LEDs operate in a regime where the pump should be optimized for a short rise time and high peak intensity, whereas fall time and overall pulse duration are less important. Lasers pumped with this approach need to have very low thresholds which can now be routinely created using (one-dimensional) distributed feedback lasers. In this particular case stripe-shaped excitation with linearly polarized light is beneficial. Arrays of micron-sized flip-chip LEDs have been arranged in an appropriate stripe shape and the array dimensions were chosen such that the divergence of LED emission does not cause a loss in peak intensity. These micro-LED arrays have successfully been used to pump OSLs with thresholds near 300 W/cm^2 (~9 ns rise time, 35 ns pulse duration), paving the way for compact arrays of indirectly electrically pumped OSLs.

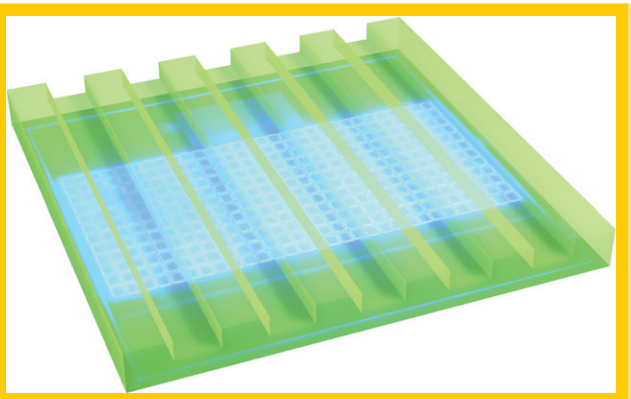

ORIGINAL PAPER

Micro-LED pumped polymer laser: A discussion of future pump sources for organic lasers

Johannes Herrnsdorf[1,*], Yue Wang[2], Jonathan J. D. McKendry[1], Zheng Gong[1], David Massoubre[1], Benoit Guilhabert[1], Georgios Tsiminis[1], Graham A. Turnbull[2], Ifor D. W. Samuel[2], Nicolas Laurand[1], Erdan Gu[1], and Martin D. Dawson[1]

1. Introduction

Organic chromophores have always played an important role in photonics. Considerable efforts are undertaken to exploit them for solid-state laser sources because they offer simple fabrication methods and access to the whole visible spectrum (including schemes for mechanical and electrical laser wavelength tuning) as well as potential for mechanically flexible devices. The challenge to achieve an electrically pumped organic solid-state laser (OSL) is a subject of ongoing research. However, enormous obstacles have to be overcome and direct electrical pumping of an OSL has not been achieved yet [1]. Therefore, this article will concentrate on optical pumping and in particular the use of GaN light-emitting diodes (LEDs) as pump sources. Such an approach aims to make a virtue of optical pumping and enable compact devices which closely mimic the properties a directly electrically driven device would have.

From this point of view there is no big difference between organic semiconductor lasers and lasers based on dye-doped transparent polymers. Hence, the acronym "OSL" will be extended here to cover both types of devices.

Typical pump sources for OSLs are frequency-doubled or -tripled Nd:YAG lasers (532 nm or 355 nm, respectively), nitrogen lasers (337 nm), frequency doubled Ti:sapphire lasers (400 nm) and optical parametric oscillators (variable wavelength). Less common are dye lasers (wavelength depending on the dye and resonator) and frequency doubled ruby lasers (347.15 nm). All of these are very bulky systems which are often maintenance intensive and may have high acquisition and running costs, compromising the organic materials benefits. Therefore, there has been a move towards more compact sources [1]. In a first instance, these were diode-pumped passively Q-switched Nd:YAG or Nd:YVO_4 microchip lasers emitting at 355 nm or 532 nm [2, 3].

Further simplification can be achieved by directly pumping the OSL with an electrically driven inorganic semiconductor device, i.e. either a laser diode (LD) or a light-emitting diode (LED). Owing to the recent advances in GaN based material growth and processing, driven by the prospect of solid state lighting and high density data storage, GaN LDs (400–450 nm) were proven to be suitable pump sources for OSLs by various groups [4–11]. A relatively unexplored area is the use of GaN LEDs as pump

[1] Institute of Photonics, University of Strathclyde, Glasgow G4 0NW, UK
[2] Organic Semiconductor Centre, School of Physics and Astronomy, University of St. Andrews,, St. Andrews KY16 9SS, UK
*Corresponding author: e-mail: johannes.herrnsdorf@strath.ac.uk

sources. Prior to the work presented here, only a few proof-of-concept reports of LED-pumping have been published based on commercial high power LEDs that allow excitation intensities up to 1 kW/cm^2 [12–14].

In this report, we present the systematic improvement of organic lasers and pumping conditions with the particular objective to use arrays of micron-sized flip-chip GaN LEDs [15, 16] as pump source. This LED format was chosen because it holds potential for enhanced functionality in future devices such as pattern programmability and potential for integration with CMOS control electronics [16]. As an outcome of this work, OSLs with thresholds competitive to the best values reported so far could routinely be created and a micro-LED array pumped OSL was achieved. The lasers used a distributed feedback (DFB) cavity and it is shown that in this case an elongated excitation spot of several mm length and a few hundred μm width is beneficial compared to a symmetrical pump spot. Consequently, the dimensions of the micro-LED array for OSL pumping were chosen to yield an appropriate stripe shape. These results are presented within the frame of a review of the basic physics relevant for the choice of pumping conditions and comparison to previous results in the literature. An important finding is that optical pulses delivered by LEDs are in a regime where the pulse rise time and peak intensity are crucial parameters, which is different compared to the case of conventional pumping by solid state lasers.

Section 2 reviews how the dynamics of the gain material influence the threshold condition. Such work was initially done for flash-lamp pumped dye lasers [17] and has seen some renewed interest with the latest developments towards continuous wave (CW) OSLs [9]. However, it has not been paid great attention when solid-state lasers were widely used as pump sources. We find here that in the case of GaN based pumping not only the pump pulse duration but also the pulse shape are important factors.

Our developments of micro-LEDs and OSLs for hybrid laser devices are presented in Sections 3 and 4, respectively. Issues arising from the divergent nature of the LED emission are discussed and we describe how the threshold condition of OSLs can be matched. This effort led to the demonstration of an OSL pumped by micro-LEDs.

2. Gain Dynamics in Organic Gain Media

This section provides crucial insight into the pumping conditions when using semiconductor based pump sources, in particular LEDs. So far, organic lasers are operated using pulsed optical pumping. This is due to the build-up of triplet-state excitons in the organic molecules that cause additional losses and prevent population inversion under CW pumping [1, 18, 19].

Most OSL research is done with pulses that are a few ns or shorter in duration. However, newly upcoming pump sources such as LDs and LEDs may operate in a different regime. An example of a high peak power optical pulse emitted by an LED is shown in Fig. 1. These pulses are

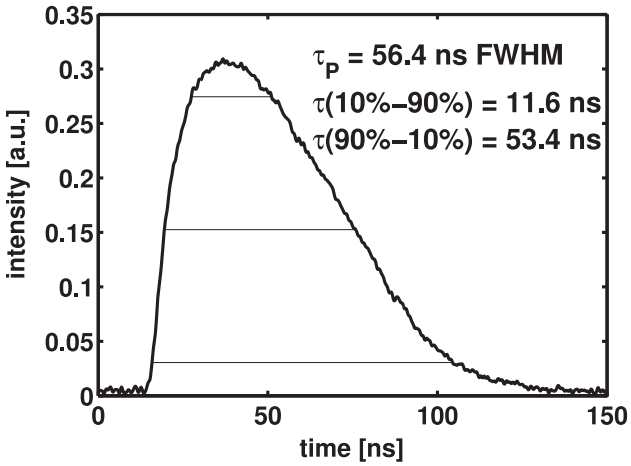

Figure 1 Typical temporal shape of an optical pulse from a GaN LED driven with a Directed Energy Inc. PCO-7110-120-15 driver.

asymmetrical with rise times around 10 ns and several tens of ns fall times. More details on how such pulses are obtained and how the pulse shape depends on the driving conditions are discussed below in Sections 2.5 and 3.3. This section provides a rate equation analysis of various pumping conditions to develop an understanding of how different pump pulse durations and pulse shapes affect the achievable optical gain and in particular the threshold.

Gain in organic materials has been achieved with pump pulse durations spanning several orders of magnitude, from femtoseconds to microseconds. Consequently, pump thresholds given in the literature are not consistently quoted in the same units. In particular, thresholds are commonly measured either in terms of fluence (energy per pulse per unit area, [μJ/cm^2]) or peak intensity [W/cm^2]. Another role for this section is to clarify how these two measures relate to each other in various pulse duration regimes.

2.1. Relevant Parameters

Obviously, very important parameters are the timescales: the singlet and triplet state lifetimes, τ_S and τ_T, the intersystem crossing rate, $k_{ST} = 1/\tau_{ST}$, and the pump pulse duration τ_{pulse}. The singlet lifetime is typically of the order of 1 ns, τ_T is significantly longer, at least a microsecond and up to milliseconds. The exact value is probably irrelevant because in any case it is orders of magnitude longer than the timescale considered here. Intersystem crossing rates have only been measured for a selected number of materials (e.g. R6G [17] and PFO [20]) and based on these it seems reasonable to assume $\tau_{ST} \approx 10 \cdot \tau_S$. Important parameters for the optical gain are the absorption cross sections of the ground- and triplet-states at the laser line, σ_0 and σ_T, (it is assumed that singlet state absorption is negligible compared to these two) and the cross section for stimulated emission, σ_L. All these parameters are illustrated in the Jablonski diagram in Fig. 2.

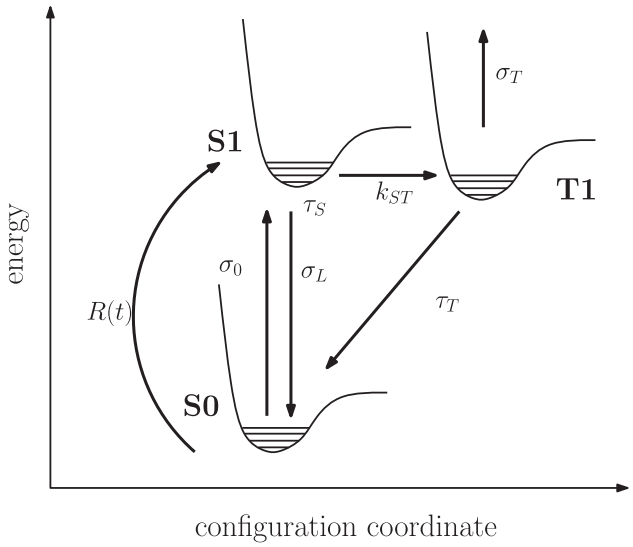

Figure 2 Jablonski diagram, illustrating the key parameters used: σ_0 and σ_T are the absorption cross sections of the ground and the triplet state at the laser line. σ_L is the stimulated emission cross section. τ_S and τ_T are the singlet and triplet state life times and $k_{ST} = 1/\tau_{ST}$ is the intersystem crossing rate. $R(t)$ is the pump rate, given by the incident pump pulse.

The system is driven by a time-dependent pump rate $R(t)$. The pump pulse duration is one of the key parameters examined here and may consist of asymmetric rise and fall times $\tau_{rise} + \tau_{fall} = \tau_{pulse}$. Note that for the theoretical calculations τ_{rise} and τ_{fall} are taken as half width half maximum to each side of the pump pulse peak. Experimentally they may also be measured as the time it takes to rise from 10 % to 90 % of the peak power (or vice versa for the fall time).

2.2. Details of the Model

The calculation follows a rate equation model by Weber and Bass [17] and an illustration of the transitions considered in this model can be found in Fig. 2:

$$\frac{\mathrm{d}N_S}{\mathrm{d}t} = -\frac{1}{\tau_S}N_S + R(t)N_0 \tag{1a}$$

$$\frac{\mathrm{d}N_T}{\mathrm{d}t} = -\frac{1}{\tau_T}N_T + k_{ST}N_S \tag{1b}$$

$$\frac{\mathrm{d}N_0}{\mathrm{d}t} = -R(t)N_0 + \left(\frac{1}{\tau_S} - k_{ST}\right)N_S + \frac{1}{\tau_T}N_T \tag{1c}$$

where $N_{0,S,T}$ are respectively the ground, singlet and triplet state populations. Note that τ_S is the overall life-time of the singlet state, including contributions from radiative and non-radiative relaxation from the singlet state directly into the ground state (transition rates $k_{S0,r}$ and $k_{S0,nr}$) and also intersystem crossing (k_{ST}), i.e. $\tau_S = 1/(k_{S0,r} + k_{S0,nr} + k_{ST})$. By normalizing $n_0 + n_S + n_T \equiv 1$ we obtain a reduced set of rate equations:

$$\frac{\mathrm{d}n_S}{\mathrm{d}t} = -\left(\frac{1}{\tau_S} + R(t)\right)n_S - R(t)n_T + R(t) \tag{2a}$$

$$\frac{\mathrm{d}n_T}{\mathrm{d}t} = -\frac{1}{\tau_T}n_T + k_{ST}n_S \tag{2b}$$

$$n_S, n_T \in [0, 1]$$

It should be pointed out, that Eq. (2) are only useful to determine the small-signal gain g_0 (and therefore the threshold). Above threshold, stimulated emission will occur on a picosecond timescale [21]. Assuming a simple set of three cross sections $\sigma_0, \sigma_T, \sigma_L$ as explained above, we can calculate an approximation of the small signal gain:

$$g \approx (n_S + n_T - 1)\sigma_0 - n_T\sigma_T + n_S\sigma_L \tag{2}$$

For the following discussion, we normalize $\sigma_L \equiv 1$ and the relative values for the other two cross sections, σ_0 and σ_T, are roughly aligned with those published for R6G [17]. Specific values of the parameters are given in the captions of corresponding figures throughout the paper.

2.2.1. Towards CW OSLs

Pumping a dye or light-emitting polymer with a CW pump source clamps the singlet and triplet populations as given by the steady-state solution of Eq. (2):

$$\left.\frac{n_S}{n_T}\right|_{CW} = \frac{\tau_{ST}}{\tau_T} \qquad (\approx 0.01) \tag{3}$$

Such a large fraction of molecules in the triplet state will cause significant absorption which is normally prohibitive. CW operation has been obtained using a solid state organic film on a rotating disk, though it is difficult to obtain low-noise laser output due to inhomogenities in the film [22,23].

Zhang and Forrest [9] recently claimed that introducing a triplet quenching mechanism (that reduces τ_T) can be sufficient to allow CW operation from a single pump spot. They back up their claims by experimental verification that stimulated emission can occur over a duration of a few tens of micro-seconds which is orders of magnitudes longer than previously reported and possibly only limited by material degradation. It is not clear whether true CW operation can be achieved this way but the results are very encouraging. A similar experiment using very long pump pulses was reported earlier by Yamashita *et al.* [24] though their measurements lack the crucial time-resolved recording of the organic laser emission and therefore it is unknown for how long gain was really present.

As opposed to true CW operation, it is also feasible to strive for quasi-CW lasers that operate in pulsed mode but at very high repetition rates. OSL operation at 5 MHz repetition rate has indeed been reported [25] and was later attributed to the low triplet state absorption of the material that was used for this experiment [19].

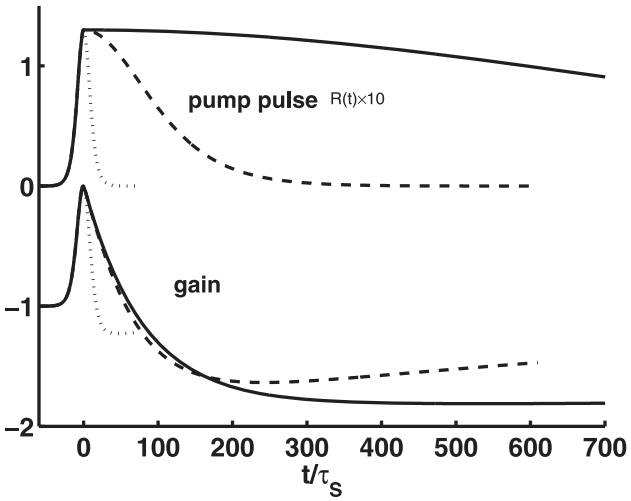

Figure 3 Time dependent pump pulse and corresponding optical gain for pulses with fixed rise time and peak intensity but different fall times at threshold. Parameters are $\tau_S = 1, \tau_{ST} = 10, \tau_T = 1000, \tau_{rise} = 10, \sigma_T = 2, \sigma_0 = 1, \sigma_L = 1$. The fall times are $\tau_{fall} = 10, 100, 1000$.

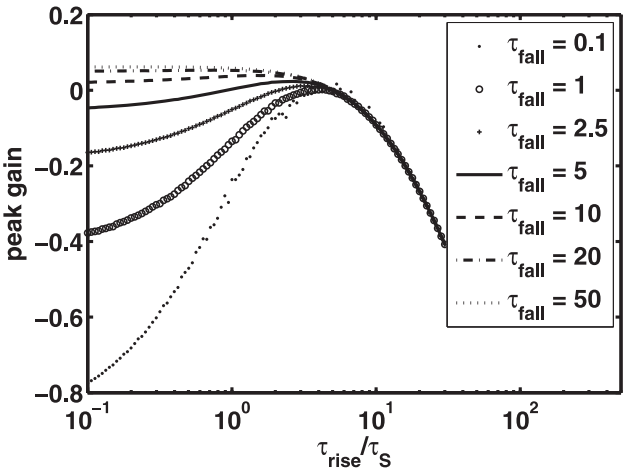

Figure 4 Maximum gain as a function of rise time at constant pump peak intensity and various fall times. Parameters are $R_{max} = 0.115, \tau_S = 1, \tau_T = 1000, \tau_{rise} = 10, \sigma_T = 2, \sigma_0 = 1, \sigma_L = 1$.

2.3. Optical Gain under Pulsed Pumping

Rate Eq. (2) were solved numerically for sech^2 shaped pump pulses with a peak pump rate of R_{max} (τ_{pulse} is treated as FWHM, hence the factor 1.76):

$$R(t) = R_{max} \cdot \mathrm{sech}^2\left(1.76\frac{t}{\tau_{pulse}}\right) \tag{4}$$

or in case of asymmetrical pulses:

$$R(t) = R_{max} \cdot \begin{cases} \mathrm{sech}^2\left(0.88\frac{t}{\tau_{rise}}\right), t < 0 \\ \mathrm{sech}^2\left(0.88\frac{t}{\tau_{fall}}\right), t \geq 0 \end{cases} \tag{5}$$

The populations found this way are then fed into Eq. (2).

As a first illustration of how the gain in organics evolves, Fig. 3 shows the temporal evolution of the pump rate and gain for asymmetrical pump pulses according to Eq. (5) in a regime of relatively long rise time (longer than the singlet state lifetime) and even longer fall times. The peak intensity and rise time has been kept constant but the fall time and thus the pump fluence was changed. It can be seen that for all of the pump pulses the gain just about reaches transparency, i.e. all pulses are at threshold. Hence we conclude that in this regime, a consistent measure for threshold is the peak intensity while the threshold fluence will vary strongly.

To investigate further the influence of the rise time, we record the maximum gain obtained during the pulse and plot it as a function of the rise time. This is done in Fig. 4 where the pump rate was chosen such that the best cases are just above threshold. It can be seen that for fall times longer than τ_{ST} it is only the rise time that governs the gain and not the overall pulse duration. In this case of long fall time the peak intensity is the most important figure of merit for the threshold condition, in particular when the rise time is at the order of or shorter than τ_S.

On the other hand, we expect *a priori* that for very short pulses the pump fluence is the relevant parameter. Hence, with increasing pulse duration there has to be a transition regime until we are in a regime as above where the peak intensity is more relevant. This transition is studied with symmetrical pulses. Figure 5 shows the maximum gain achieved depending on the pump pulse duration. In the top graph, the pump fluence was fixed to a value just above the lowest threshold (in terms of fluence). We see that above $0.01 \cdot \tau_S$ the maximum gain drops off with increasing pulse duration but it is constant below. Hence, for very short pulses the maximum gain (for a given fluence) and therefore also the threshold fluence are the same irrespective of pump pulse duration. The bottom graph in Fig. 5 is similar but for fixed pump peak intensity. We see that the gain and thus the threshold depends strongly on the pump pulse duration. For pulses longer than $0.01 \cdot \tau_S$ both threshold values, threshold fluence and threshold peak intensity, depend on the pump pulse duration and fair comparisons can be very difficult. Note that for the longest pulses in this graph it is effectively the rise time only that governs how much gain is obtained.

2.4. Different Regimes of OSL Pumping

In general, neither the fluence nor the peak intensity are good measures of threshold by themselves. Both values should always be provided (or at least the pump pulse duration should be specified) in order to allow fair comparison and even then the exact pulse shape may have a significant influence. In particular, the following regimes have been identified:

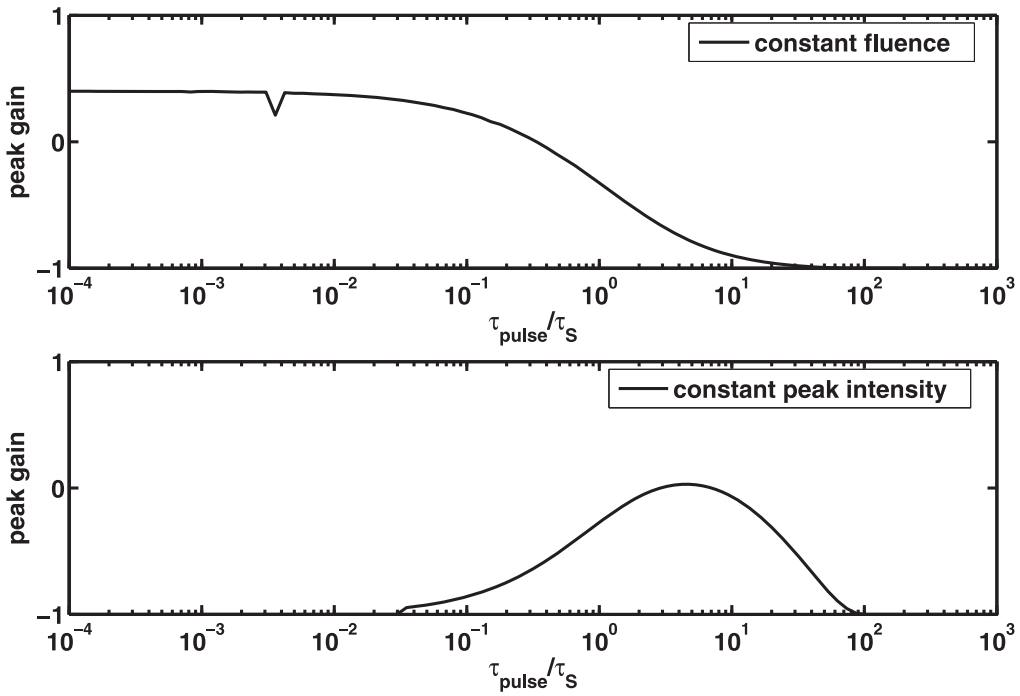

Figure 5 *Top*: maximum optical gain depending on the pulse duration for a fixed pulse fluence ($R_{max} \cdot \tau_{pulse} = 0.12$). The dip in the graph is caused by numerical error. *Bottom*: maximum optical gain depending on the pulse duration for a fixed peak intensity ($R_{max} = 0.13$). Parameters are $\tau_S = 1$, $\tau_T = 1000$, $\tau_{rise} = 10$, $\sigma_T = 2$, $\sigma_0 = 1$, $\sigma_L = 1$.

1. **Short pulse**
   τ_{pulse} about two (or more) orders of magnitude smaller than τ_S:
   In this case the threshold fluence is the relevant measure and is independent of the pulse duration.
2. **Short rise time, long fall time**
   Asymmetrical pulse with long fall time, $\tau_{fall} > \tau_{ST}$, and τ_{rise} on the order of or shorter than τ_S:
   In this case the peak intensity is a good and consistent measure for threshold. Overall pulse duration and threshold pump fluence are unimportant to the laser threshold.
3. a) **Medium rise time, long fall time**
   $\tau_{fall} > \tau_{ST}$, $\tau_{rise} > \tau_S$, $\tau_{rise} < \tau_{ST}$:
   In this case the peak intensity is a good measure for threshold but depends strongly on the rise time (the shorter, the better). Overall pulse duration and threshold pump fluence are unimportant.
   b) **Long rise time (fall time irrelevant)**
   Fixed rise time on the order of τ_{ST} or longer:
   In this case the peak intensity is a good measure for threshold but depends strongly on the rise time (shorter rise times give lower thresholds). Fall time, overall pulse duration and threshold pump fluence are not important.
4. **Medium rise and fall times**
   $\tau_{pulse} > 0.01 \cdot \tau_S$ but neither $\tau_{rise} > \tau_{ST}$ nor $\tau_{fall} > \tau_{ST}$:
   This is the somewhat unfortunate regime, where neither the threshold fluence nor the threshold peak intensity are really consistent measures in any way. Comparison of results - different pump lasers or even different materials pumped by the same laser - are notoriously problematic and only order-of-magnitude differences can clearly be classed as meaningful.

Only regimes 1 and 2 allow precise and straight forward comparisons of experiments using different materials and/or different pump sources. However, for practical reasons - in particular availability of suitable pump sources - most reported experiments were done in regime 4.

2.5. Implications for LED and LD pumping

High power optical pulses emitted by LEDs that are driven by a laser diode driver are asymmetrical. An example of such a pulse, representative for both broad-area and micro-LEDs, is given above in Fig. 1. The rise time depends on the LED itself and the driver electronics. Typical values are $\tau_{rise} \approx 10-15$ ns, see Section 3.3 below for more details. The rise time appears to stay fixed, independent of the peak current delivered by the driver. However, the fall time changes dramatically with drive current. Values from 10 ns just above turn on up to more than 50 ns at several kA/cm^2 have been observed. An example of how the optical pulse duration depends on the peak LED current is given in Fig. 6. The gradual increase in optical pulse duration with increasing current is solely due to increase of the fall time. Throughout the measurement, the rise time was constant

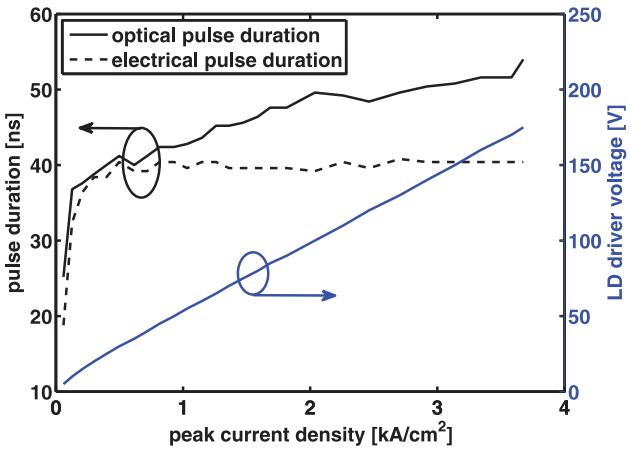

Figure 6 Optical and electrical pulse duration as a function of LED current when operating an 8×60 micro-LED array with a Directed Energy Inc. PCO-7110-120-15 LD driver. The optical pulse rise time was constant at 10 ns. For reference, the input voltage supplied to the LD driver is plotted as well.

at 10 ns. Notably, the electrical pulse assumes a constant duration shortly after turn-on, i.e. the increasing fall time is only visible in the optical pulse.

These values for τ_{rise} and τ_{fall} are to be compared with typical singlet state lifetimes on the order of $\tau_S \sim$1 ns and $\tau_{ST} \sim$10–30 ns. Therefore it is only the rise time and the peak intensity that matter whereas the variation in fall time has hardly any influence on the suitability for OSL pumping. This can be seen in Fig. 3 which in fact represents a typical LED-pumping scenario. It should in practice be aimed to have as short rise times as possible without compromising the peak intensity. To our knowledge and experience, exactly the same arguments apply also for GaN based LDs as pump sources.

3. Flip-Chip Micro-LEDs for OSL Pumping

Previous work on LED pumping of OSLs used commercially available broad-area LEDs with a size on the order of 1×1 mm^2 [12, 13]. A custom layout can be achieved by arranging micron-sized LEDs in a close-packed array of the desired dimensions. This way, the pump geometry can be optimized to match the requirements of the specific OSL used, e.g. a stripe shape in the case of one-dimensional DFB lasers as discussed below in Section 4.3. The micro-LED format also benefits from increased light extraction due to the LED side-walls and unique electrical characteristics. Generally, individual micro-LEDs can sustain significantly higher current densities than broad-area LEDs due to reduced current crowding and improved thermal properties [26]. We will show below that this advantage is compromised to some extent by effects of divergence of LED emission and the necessity to use close-packed arrays. Still, the performance of these arrays is sufficient for OSL pumping. These results are an important milestone towards a new generation of highly compact devices where each micro-pixel is driven by its own micro-driver.

In the work presented here we use arrays of square pixels with 30 μm edge length at 33 μm pitch having a fill factor of 0.83. Pixel size and spacing were chosen to allow reliable fabrication of high-quality devices limited by the precision of mask-alignment during photolithographic fabrication steps. The micro-LEDs were fabricated from commercially available wafers grown on patterned sapphire substrates (PSS). Micro-LED mesas about 1 μm high are created by inductively coupled plasma etching. The p-GaN backplane is then overcoated with a current spreading layer of NiAu alloy. Typical PSS thicknesses are around 350 μm and can be as thick as 430 μm. It is possible to thin the sapphire layer down to 150 μm without having to change the micro-LED fabrication process.

3.1. Pump Setup

When pumping OSLs with a laser the pump source can be installed remotely from the OSL and the laser beam can be directed and focused onto the sample with mirrors and lenses. However, such a setup is not appropriate for LEDs because of the highly divergent nature of their emission. It is very difficult to efficiently collect LED emission with a lens. Therefore, the highest pump power/energy densities on the organic film are obtained when the gain medium is brought in direct mechanical contact with the LED surface, or at least in as close proximity as possible. LED performance for OSL pumping is thus best characterized by the power density that can be obtained at the LED surface.

3.2. Actual Pump Spot Dimensions

The micro-LED arrays used for OSL pumping were in flip-chip format, i.e. they emit through the PSS on which the epitaxial structure was grown. Typical PSS thicknesses of 350 μm are considerably larger than the diameter of individual micro-LEDs and therefore the divergence of LED emission upon propagation through the PSS is important. For example, a single 30×30 μm^2 pixel driven on its own could give a peak intensity of 392 W/cm^2 when normalized to the active pixel area. However, due to the divergence the peak intensity at the sapphire surface in this case was only 2.45 W/cm^2. To study this effect in more detail, a Monte-Carlo ray-tracing model was employed [27]. *Ab-initio* calculations of the full LED structure are computationally expensive, and quantitatively trustworthy results require simple and well-controlled conditions [28, 29]. To obtain reliable results in the complex situation of a micro-LED array, only the propagation through the sapphire was modeled based on three simplifying assumptions:

1. Since the n-GaN and GaN buffer layers are relatively thin, it was assumed that the spatial emission profile at the GaN/sapphire interface is identical to the mesa-profile of the micro-LED array.

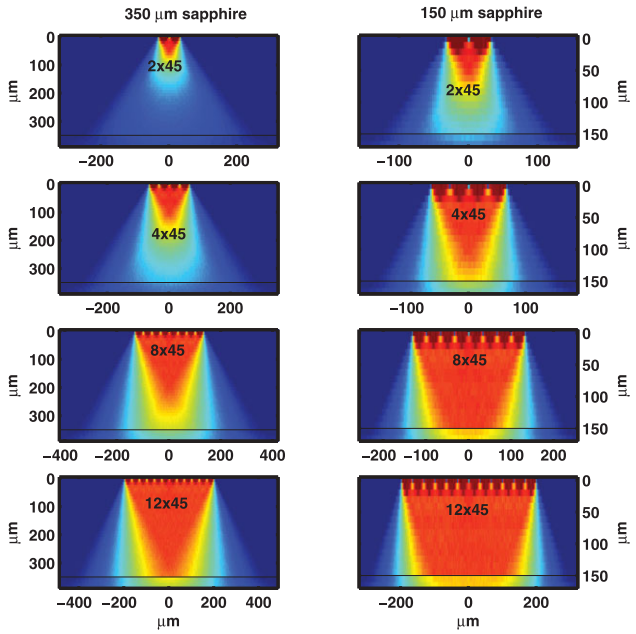

Figure 7 Calculated intensity of micro-LED light as it diverges while propagating through the sapphire window of flip-chip micro-LED arrays. The sapphire/air interface is indicated by a black line and only emission within the escape cone has been accounted for.

2. Each point at the GaN/sapphire interface has the same angular emission profile.
3. Multiple reflections between the sapphire/air and sapphire/GaN surfaces can be neglected. To properly account even for one back-reflection would be very time-consuming owing to the patterned nature of the GaN/sapphire interface.

The far-field emission profile of micro-LEDs is roughly Lambertian. On the basis of the above assumptions it is possible to recreate from Fresnel equations the angular emission profile within the sapphire for all emission within the acceptance cone. Then, a large number of point emitters at the GaN/sapphire interface are positioned randomly within the emissive area. They all have the same angular emission profile and the propagation of their emission is traced, yielding the desired spatial emission profile at the sapphire/air surface.

Figure 7 shows calculated intensity cross sections through the sapphire along the short axis of micro-LEDs arranged in stripe-format. It is clearly visible how, particularly in the case of thin stripes, the LED emission diverges strongly before reaching the sapphire/air surface. The available pump spots after passing through the sapphire/air interface are plotted in Fig. 8. From both figures it becomes clear that (in the case of square pixels) one needs at least 12 pixel wide stripes to fully mitigate the effects of divergence through 350 μm of sapphire and 8 pixels in the case of 150 μm thick sapphire. A summary of calculated stripe widths is given in Table 1. The numerical results were confirmed experimentally with a knife-edge measurement.

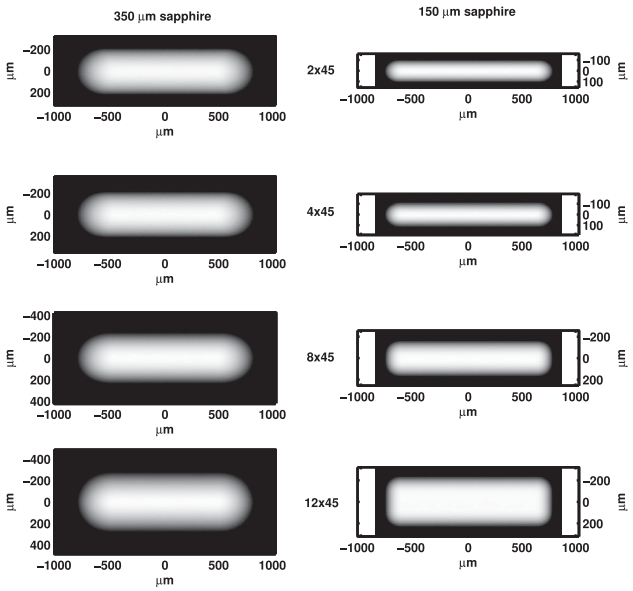

Figure 8 Calculated intensity profiles at the sapphire surface of stripe-shaped micro-LED clusters.

Table 1 Calculated stripe widths of stripe-shaped micro-LED arrays. The stripe length n in case of the actual devices used was a multiple of 30 or 45 pixels, respectively.

array	stripe width (active region) [μm]	sapphire thickness [μm]	stripe width (sapphire surface) [μm]
$2 \times n$	66	350	350
$4 \times n$	132	350	344
$8 \times n$	264	350	365
$12 \times n$	396	350	420
$2 \times n$	66	150	150
$4 \times n$	132	150	168
$8 \times n$	264	150	267
$12 \times n$	396	150	400

These were done by bringing a metal step-edge on a glass in contact with the sapphire surface and moving it across a lit up micro-LED array.

3.3. Pulsed Operation

Pulses suitable for OSL pumping are obtained by operating the LED with a LD driver. A simplified schematic of the LD driver circuit is shown in Fig. 9. As long as the switch (a metal-oxide-semiconductor field-effect transistor, MOSFET) is open and a positive voltage is applied to the high voltage input, a capacitor will be charged through an on-board diode. Upon closing of the switch, this capacitor will discharge through the LED giving rise to a short current pulse. An optional inductor can be installed in

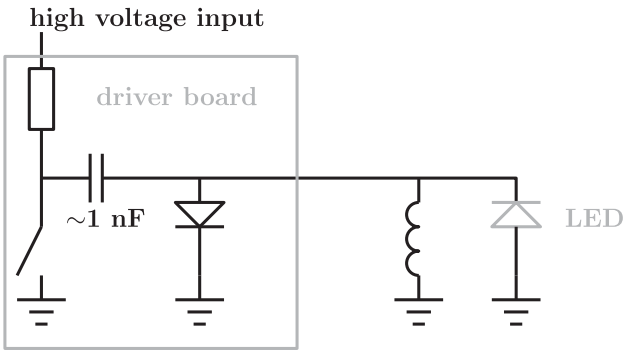

Figure 9 Schematic of the driver circuit used for pulsed driving of LEDs.

parallel to the LED for impedance matching in order to reduce unwanted current oscillations. In this setup, the pulse duration, pulse shape and peak power generally depend on the voltage supplied to the high voltage input, the capacitance that is discharged, the inductance in parallel to the LED, the switching characteristics of the MOSFET, the electrical characteristics of the LED and the external quantum efficiency (EQE) of the LED. Pulses obtained this way are several 10s of nanoseconds long (see Figs. 1 and 6) and can have peak power densities up to several hundred W/cm^2. Sub-nanosecond optical pulses from a single micro-LED were demonstrated by MOSFET-switching of a constant supply voltage [30] but at much lower peak power.

Three drivers, Directed Energy Inc. PCO-7110-120-15, PCO-7110-40-4 and PCO-7110-100-7 were used to operate the micro-LEDs. The 120-15 driver delivered the highest pulse energies in ~50 ns optical pulses. The 40-4 driver can deliver 30 ns short pulses, however typically at lower peak intensities than the 120-15 driver. The 100-7 driver is capable of delivering comparable peak intensities as the 120-15 driver in ~35 ns optical pulses. Typical rise times are 6–9 ns (40-4 and 100-7 drivers) and 10-15 ns (120-15 driver) and appear to be independent of the peak current density, whereas the fall time tends to increase with increasing peak current. Optical pulse durations were measured by a photomultiplier tube (PMT) or a fast photodiode connected to an oscilloscope with 500 MHz bandwidth. Electrical pulses were monitored with an oscilloscope current probe.

The voltage supplied to the driver can be up to 495 V depending on the driver used. Above, in Fig. 6 the properties of the electrical pulses obtained this way are shown. Devices turn on near 5 V and at about 3× this pulsed turn on voltage the electrical pulse duration assumes a constant value. For OSL pumping, the device has to be operated orders of magnitude above turn-on.

3.4. Micro-LED Performance

Under pulsed driving, GaN micro-LEDs can sustain very high peak electrical currents up to several kA/cm^2. In these conditions, the optical power density at the sapphire surface can reach several hundred W/cm^2, which is in principle sufficient for OSL pumping. A number of arrays emitting at 450 nm achieved peak intensities ranging from 180–290 W/cm^2 obtained with both the 120-15 or the 100-7 drivers and the best performing arrays were capable of delivering up to 345 W/cm^2. The best performance of an micro-LED array emitting at 405 nm was 123 W/cm^2 in a 55 ns optical pulse driven by the 120-15 driver.

3.4.1. Limitation of LED Pulsed Output

When driving an LED with a DC voltage the light intensity will peak at a certain current and stagnate or even drop if the current is further increased. This roll-over is normally reversible if the current was never pushed significantly beyond the roll-over point. In pulsed operation however, no such roll-over was observed and the micro- LEDs could be damaged irreversibly in a very sudden manner. In a few cases, damage occurred at the wire bond pads resulting in detachment of the wire from the pad. It is believed that connecting two or three wires to each pad reduces the risk of this happening. The most common type of damage however is the sudden occurrence of a current leak. In pulsed L-I curves, such an event manifests in a sudden drop of optical pulse energy. Once such damage has occurred, pulsed device performance remains significantly inferior than prior to the event and a strong leakage current is observed in DC operation. It was also observed that no well-defined damage threshold exists. Damage may occur after a large number of pulses has already been applied at constant driving conditions.

It is known that in the regime of high current densities LEDs tend to suffer from an effect called “current crowding” [31,32], i.e. the electric current is not spread uniformly across the LED area. Micrographs shown in Fig. 10 show that micro-LED arrays which light up uniformly in DC operation show significant current crowding towards the n-contact when driven in pulsed mode at a few kA/cm^2 peak current density. Figure 10 also shows a micrograph of a damaged micro-LED array where the damaged area can clearly be associated with the area of highest current density. It has to be noted though that in most cases the damaged region cannot be clearly identified under a microscope. Effects of current crowing can be reduced by optimized layout of contacts [33].

3.5. Summary of micro-LED Performance

To be able to pump lasers with a micro-LED array, the micro-LEDs have to be operated with very high peak current densities of several kA/cm^2. The driver has to be chosen appropriately to enable such high currents with a rise time as short as possible (~6–9 ns in our case). A major limitation of micro-LED performance in this configuration appears to be the occurrence of current leaks, probably associated with current crowding effects. Furthermore, the divergent nature of the LED emission has to be taken care of when choosing

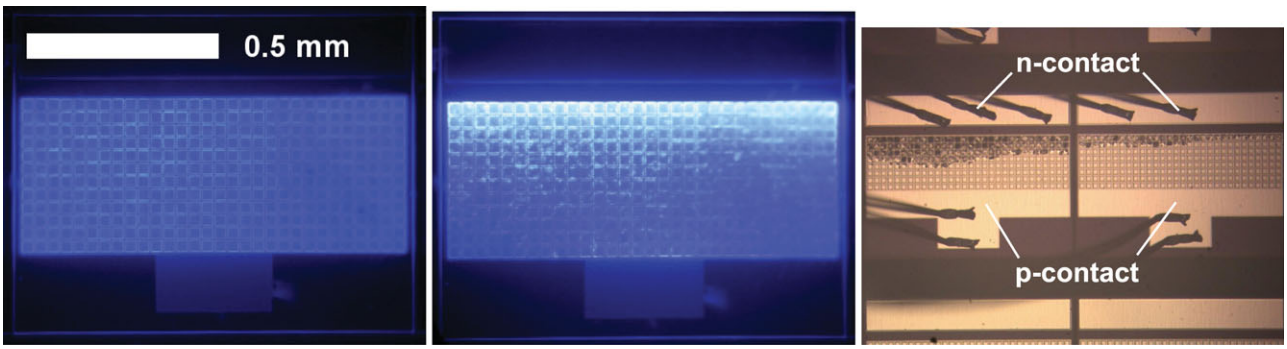

Figure 10 *Left*: Optical micro-graph of a micro-LED array under CW driving (<10 A/cm^2). *Middle*: The same stripe under pulsed pumping (2 kA/cm^2 peak current in 55 ns pulses). *Right*: Optical micrograph of micro-LED arrays that were damaged during pulsed operation.

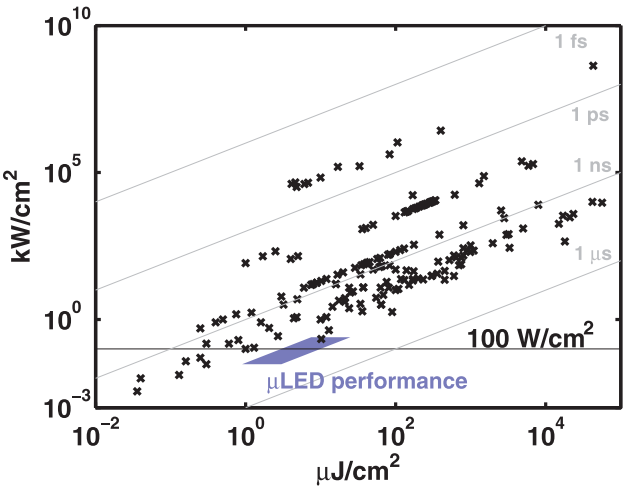

Figure 11 Summary of reported organic DFB laser thresholds. For reference, the typical regime of GaN flip-chip micro-LED performance in pulsed operation is highlighted. The grey lines indicate constant pump pulse durations. Compare also Fig. 15.

the device geometry. Stripe-shaped arrays of close-packed 30 × 30 μm flip-chip micro-LEDs with stripe dimensions of ∼400 μm width and several mm length have suitable characteristics for OSL pumping with a pump wavelength of 450 nm.

For comparison with OSL performance, the typical regime of micro-LED operation (30-250 W/cm^2 peak intensity, 30-100 ns optical pulse duration) is indicated below in Figs. 11 and 15.

4. Organic Lasers for Integration with LEDs

As opposed to laser sources, LEDs have a highly divergent light emission, making it difficult to efficiently achieve a high excitation density in the gain materials. Therefore, lasers suitable for LED pumping should ideally be characterized by a low threshold. In this section, efforts made to consistently fabricate OSLs with performance suitable for LED pumping are presented and compared to state of the art performance reported in the literature. The literature values plotted in the figures are taken from an extensive literature review on OSL characteristics [27].

4.1. Laser Thresholds

Thresholds are typically recorded as either threshold pump fluences (F_{th}, measured in μJ/cm^2) or as threshold pump intensities (I_{th}, measured in kW/cm^2). It was pointed out above in Section 2 that in most cases neither value is meaningful on its own and both should be specified. Threshold values of organic lasers reported in the literature [27] are plotted in Fig. 11. In general, a massive spread of thresholds over many orders of magnitude has been reported. Interestingly, the lowest thresholds in terms of both fluence and intensity were obtained with few-nanosecond pump pulses. GaN LEDs can deliver a few hundred W/cm^2 in pulses of several 10 ns duration, as indicated in Fig. 11. So far, this regime is only reached by the cutting edge of organic laser technology and it is therefore important to develop fabrication techniques that allow creating lasers with such low threshold reliably and routinely. Two reasons in particular may be responsible for the lack of data points in the LED pumping regime in Fig. 11. First of all, GaN light sources (LDs and LEDs) with attractive characteristics for OSL pumping have only recently become available and were only used in a limited number of publications. The majority of reports use nano-second pulsed solid-state or gas lasers that have different optical pulse durations and shapes than LDs or LEDs. Furthermore, as explained in Section 2, LEDs operate in a regime where the optical pulse rise time is crucial. So far no optimization for this aspect has been reported except for flashlamp-pumped dye-lasers.

4.1.1. Outstandingly low thresholds

LEDs typically deliver a few 100 W/cm^2 peak intensity with fairly long rise times on the order of 10 ns. Direct comparison with solid state laser pumping is not straight-forward

but generally an OSL suitable for LED pumping needs to have a threshold of this magnitude or lower. In fact, very few OSLs with such performance were achieved so far. Within about 200 publications on OSLs [27], only six devices with threshold below 100W/cm^2 have been reported [34–39] with the lowest reported threshold to our knowledge being 36nJ/cm^2 (3.6W/cm^2) obtained with a fluorene-copolymer and a mixed order grating [37]. There are also further reports of thresholds below 250W/cm^2 [12,40–42]. We demonstrate below that - despite most thresholds reported being significantly higher - current state-of-the-art in OSL fabrication allows reliable creation of lasers with sub-100 W/cm^2 thresholds (4 ns pump pulses).

Notably, all the above mentioned lasers are distributed feedback (DFB) lasers. Reported thresholds for other cavity-types are significantly higher. Probably the most outstanding result in terms of W/cm^2 is a micro-cone laser tested with two different pump sources yielding thresholds of 3.5μJ/cm^2 (> 700W/cm^2) and 16μJ/cm^2 (800W/cm^2), respectively [10]. Furthermore, a very low threshold fluence of 220 nJ/cm^2 (1470 kW/cm^2) was recently reported for fs-excitation of organic semiconductor slab nanocrystals [43]. Thresholds in the range 1–10 μJ/cm^2 and 1–10 kW/cm^2 have been achieved in slab waveguides with high quality facets [44, 45] and distributed Bragg reflector lasers [5, 41, 46]. Given that these values are an order of magnitude higher than the best DFB lasers, it has to be concluded that the DFB-structures are currently the most suitable cavity layout for low-threshold OSLs.

4.2. Material Choice

The efficiency and available output power of GaN based emitters depends strongly on the emission wavelength of the device. Blue devices at 450 nm perform significantly better than green- or near-ultraviolet emitting devices [47]. Therefore, the absorption of the organic gain material should be matched for pumping at 450 nm. It should be noted, that some of the lowest thresholds reported so far were achieved with blue-emitters that absorb in the near-UV [37]. Therefore, these devices may not be suitable for LED-pumping despite their extraordinarily low thresholds. As gain material for the work presented here, we use Poly[2,5-bis(2′,5′-bis(2″-ethylhexyloxy)phenyl)-p-phenylenevinylene] (BBEHP-PPV) [35] which has an absorption peak near 430 nm and delivers optical gain around 535 nm [13, 48].

4.3. Pump Spot Geometry and Pump Polarization

Excitation areas used for OSL experiments in the literature span several orders of magnitude with the smallest to our knowledge being a circle of 4 μm diameter [49] and the largest 3 mm × 2.5 cm [46]. However very little systematic optimization of the pump geometry has been reported [50]. Particularly in the case of (one-dimensional) DFB lasers it may be expected to have a strong impact on the performance because the DFB grating and slab waveguide geometry impose preferred propagation and polarization directions. Laser light will propagate perpendicularly to the grating grooves because only then optical feedback is present and therefore a pump stripe aligned with the propagation direction should be beneficial. Furthermore, the grating is normally designed such that it provides feedback at the laser wavelength for the fundamental TE_0 polarization mode of the slab waveguide (which also has the best spatial overlap with the gain region) whereas the feedback for other polarization modes is at wavelengths that have significantly less or even no optical gain. Therefore, the laser emission of such a laser is linearly polarized which also has implications on the ideal pumping conditions.

To prove that a TE-polarized elongated excitation spot aligned perpendicularly to the grating grooves is beneficial for DFB laser pumping, devices were created by spin-coating BBEHP-PPV onto a polymer grating with 340 nm period. These lasers were excited with a 0.3 × 3 mm^2 pump stripe and the linearly polarized UV light from a frequency-tripled Nd:YAG pump laser could be rotated by a $\lambda/2$-waveplate. Figure 12 illustrates the possible configurations of stripe alignment and polarization.

Power transfer functions of each configuration are shown in Fig. 12. It can generally be seen, that pumping in the $\perp$ geometry leads to lower threshold than pumping in the $\parallel$ direction. This can readily be explained by the fact that the laser mode propagates in the $\perp$-direction and thus is supplied with gain over a longer propagation length when pumped in the $\perp$ geometry. Also, gain-guiding may help optical confinement to the laser mode. This latter aspect is supported by the observation that laser thresholds tend to be slightly lower when pumped with 0.3 mm broad stripe as compared to pumping with a 3 × 4.5 mm^2 pump spot (e.g. 7.9μJ/cm^2 (1.58 kW/cm^2) using the 1:10 elongated stripe compared to 11.7μJ/cm^2 using the bigger 2:1 pump spot).

In terms of pump polarization, it can be seen from Fig. 12 that both threshold and slope efficiency are superior when the pump is TE-polarized compared to the TM' case. The interpretation is that linearly polarised pump light preferentially excites molecules that are aligned in a certain direction such that their dipole moment is parallel to the pump electric field vector. These molecules will give a stronger contribution to the gain of the laser mode if this dipole moment is also parallel to the laser mode polarization. This is the case for TE pumping but not for TM' pumping.

The influence of pump stripe length was investigated in a similar fashion to the recent study by Calzado *et al.* [50]. Low-threshold devices (suitable for LED-pumping) - where the BBEHP-PPV was spin-coated onto large area silica gratings with 350 nm period - were excited with 4 ns pump pulses at 450 nm in a stripe of variable length. In this case a threshold reduction by an order of magnitude could be achieved by using sufficiently long stripes as is

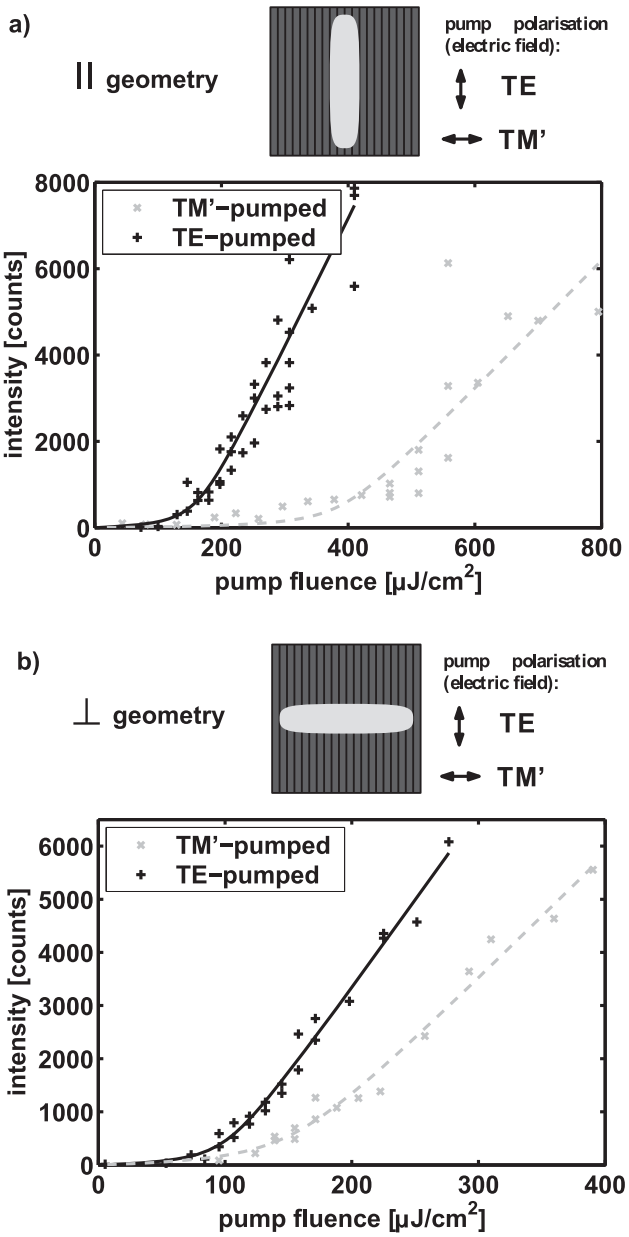

Figure 12 DFB laser transfer functions using the different pump configurations: *a*) pump stripe aligned parallel to the DFB grating grooves and *b*) pump stripe aligned perpendicularly to the grating grooves. On top of the graphs, the alignment of the stripe and the polarization direction of the linearly polarized pump light are illustrated. The solid and dashed lines are fits of the data with a soft threshold model [51].

shown in Fig. 13. This dependence of the pump threshold on the excitation stripe length is observed in both amplified spontaneous emission (ASE) on smooth silica substrates and DFB laser action on the silica gratings. The lowest threshold of a BBEHP-PPV laser we have achieved so far is 30 W/cm^2 (0.12 μJ/cm^2) from a second order DFB laser pumped by a 4 mm long and 0.4 mm wide stripe.

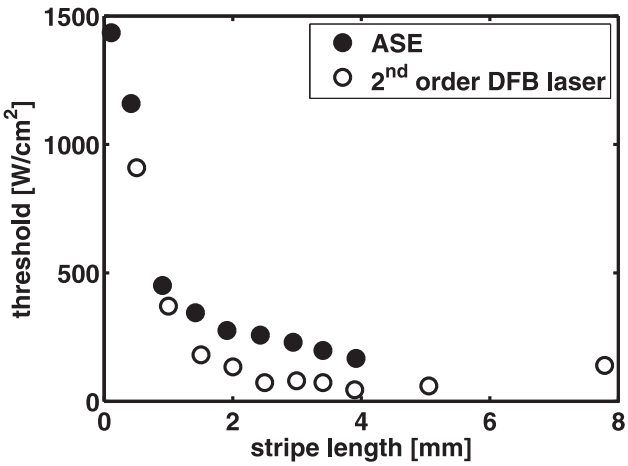

Figure 13 Pump thresholds of ASE from a BEHP-PPV film on unpatterned glass and of a second order DFB laser on silica as a function of stripe length when pumped by a stripe of 400 μm width.

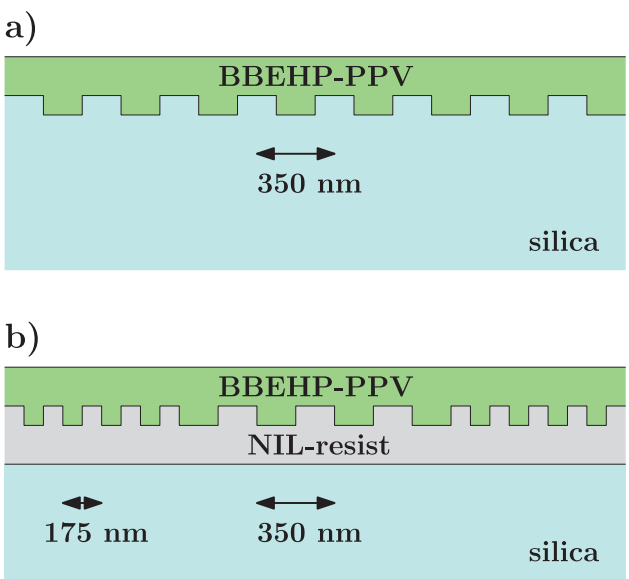

Figure 14 Schematics of BBEHP-PPV based DFB laser structures that yielded low pump thresholds suitable for LED pumping. *a*) Second order DFB laser on silica, *b*) mixed order NIL grating DFB laser.

4.4. Low-threshold OSLs for LED Pumping

Two types of BBEHP-PPV based DFB lasers were studied for possible micro-LED pumping. The first structure is a "standard" second order grating patterned directly into silica. Alternatively, a mixed order grating with 15 or 30 periods of second order in the center enclosed by first order gratings was created by nanoimprint lithography (NIL). Both structures are illustrated in Fig. 14.

Laser properties were assessed initially by pumping with an optical parametric oscillator (OPO) delivering 4 ns pulses at 450 nm wavelength. Both laser geometries allowed

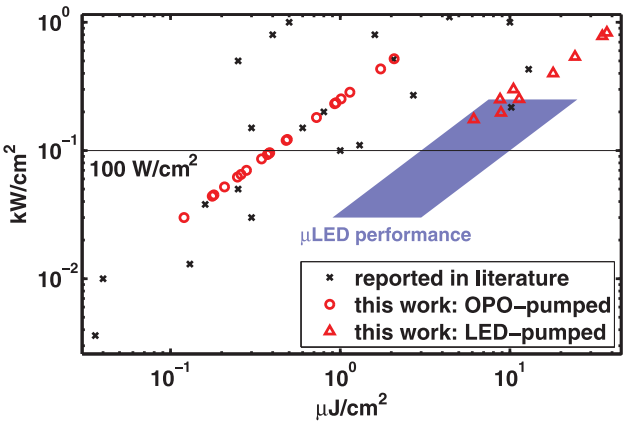

Figure 15 Thresholds of the BBEHP-PPV based DFB lasers used in this work compared to the the most outstanding results reported in the literature. Similar to Fig. 11 typical micro-LED performance is indicated.

Table 2 Comparison of BBEHP-PPV laser thresholds when pumped by an OPO (4 ns pulses) or a broad-area LED (45 ns pulses). See Fig. 14 for schematics of the device structures.

Grating	OPO-threshold [W/cm^2]	LED-threshold [W/cm^2]
2nd order	122	538
mixed order, 30 2nd order periods	57	208
mixed order, 15 2nd order periods	50	197

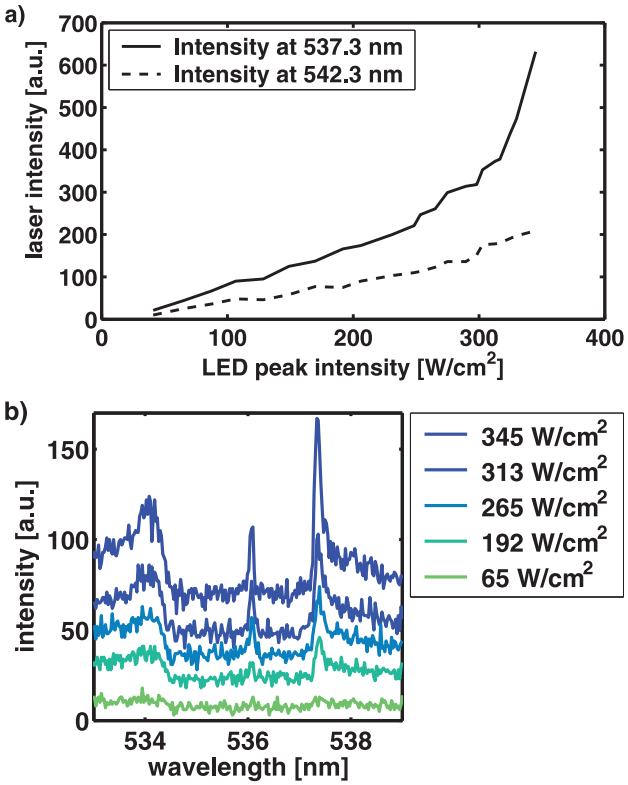

Figure 16 *a*) Power transfer function of a mixed order BBEHP-PPV DFB laser emitting at 537.3 nm pumped by a micro-LED array (8 × 90 square pixels). For reference, the power transfer function of the photoluminescence with a wavelength different from the laser line is included as well. *b*) Spectral evolution of the laser emission with increasing pump power.

reliable fabrication of OSLs with threshold peak intensities at or below 100 W/cm^2 which is competitive to the most outstanding results reported in the literature. An overview of these achievements in relation to previous results is provided in Fig. 15. Figure 15 also includes thresholds when pumping with micro- and commercially available broad-area LEDs. It can be seen that the different pulse duration of LEDs compared to the OPO has a strong impact on the threshold which is probably mainly caused by the longer rise time. The threshold peak intensity of LED-pumped lasers (~45 ns pump pulse) is typically 3–4 times higher than the in case of OPO-pumping of the same device. Examples for illustration are given in Table 2.

Successful micro-LED pumping of BBEHP-PPV mixed order DFB lasers (Fig. 14b) has been achieved in three cases above pump thresholds of 250, 175 and 300 W/cm^2. In all three cases, the micro-LED array was driven by a PCO-7110-100-7 driver, taking advantage of its shorter rise time compared to the 120-15 driver. One example of these is given in Fig. 16. In the spectra shown in Fig. 16b), the appearance of a narrow-linewidth emission peak at the long-wavelength edge of the DFB stop-band can be seen. The power transfer function of this peak is plotted in Fig. 16a) exhibiting typical laser threshold behavior at 300 W/cm^2. Laser operation at 537.3 nm is consistent with characterisation of the same OSL using OPO-pumping

5. Conclusion

Various aspects of optical pumping conditions of OSLs have been discussed with particular emphasis on using GaN LEDs as pump sources. Simulation results show that not only the pump pulse duration but also the pulse shape and in particular its rise time have a strong influence on the laser threshold. In the regime of LED pumping, optimization for a short rise time is desirable and has been achieved here by appropriate choice of the LD driver used to operate the LED. Currently achievable performance from GaN LEDs requires very low OSL threshold. It is shown that such low threshold lasers can routinely be fabricated in DFB format. In this case, optimal pumping is done with a TE-polarized pump stripe of a few hundred μm width and a few mm length which is aligned perpendicularly to the grating grooves. Consequently, flip-chip micro-LED arrays in stripe format were successfully used to pump OSLs. Also, effects of the divergence of the LED emission which are of particular importance for flip-chip micro-LEDs were

discussed. In this case, the emission of single pixels suffers too much from divergence to allow OSL pumping and arrays of multiple close-packed pixels are needed. These results are an important step towards highly functional micro-LED based devices. More generally, our findings may serve as a useful guideline for future developments of compact and practical pump sources for OSLs.

Acknowledgement. Funding for this work was provided by EPSRC under the grant EP/F05999X/1, "HYPIX", http://hypix.photonics.ac.uk/. We thank P. J. Skabara and A. L. Kanibolotsky for synthesis of the BBEHP-PPV.

Received: 29 July 2013, **Accepted:** 26 August 2013

Published online: 19 September 2013

Key words: Organic semiconductor laser, light-emitting diode, indirect electrical pumping, hybrid organic/inorganic optoelectronics.

References

[1] S. Chénais, and S. Forget, Polym. Int. **61**(3), 390–506 (2012).
[2] S. Riechel, U. Lemmer, J. Feldmann, S. Berleb, A. G. Mückl, W. Brütting, A. Gombert, and V. Wittwer, Opt. Lett. **26**(9), 593–595 (2001).
[3] G. A. Turnbull, P. Andrew, W. L. Barnes, and I. D. W. Samuel, Appl. Phys. Lett. **82**(3), 313–315 (2003).
[4] T. Riedl, T. Rabe, H. H. Johannes, W. Kowalsky, J. Wang, T. Weimann, P. Hinze, B. Nehls, T. Farrell, and U. Scherf, Appl. Phys. Lett. **88**, 241116 (2006).
[5] A. E. Vasdekis, G. Tsiminis, J. C. Ribierre, L. O. Faolain, T. F. Krauss, G. A. Turnbull, and I. D. W. Samuel, Opt. Express **14**(20), 9211–9216 (2006).
[6] C. Karnutsch, M. Stroisch, M. Punke, U. Lemmer, J. Wang, and T. Weimann, IEEE Photon. Technol. Lett. **19**(10), 741–743 (2007).
[7] H. Sakata, K. Yamashita, H. Takeuchi, and M. Tomiki, Appl. Phys. B **92**, 243–246 (2008).
[8] H. Matsuura, M. Fukuda, and H. Sakata, Laser Phys. Lett. **6**(3), 194–197 (2009).
[9] Y. Zhang and S. R. Forrest, Phys. Rev. B **84**, 241301 (2011).
[10] S. Klinkhammer, T. Großmann, K. Lüll, M. Hauser, C. Vannahme, T. Mappes, H. Kalt, and U. Lemmer, IEEE Photon. Technol. Lett. **23**(8), 489–491 (2011).
[11] S. Klinkhammer, X. Liu, K. Huska, Y. Shen, S. Vanderheiden, S. Valouch, C. Vannahme, S. Bräse, T. Mappes, and U. Lemmer, Opt. Express **20**(6), 6357–6364 (2012).
[12] Y. Yang, G. A. Turnbull, and I. D. W. Samuel, Appl. Phys. Lett. **92**, 163306 (2008).
[13] G. Tsiminis, Y. Wang, A. L. Kanibilotsky, A. R. Inigo, P. J. Skabara, I. D. W. Samuel, and G. A. Turnbull, Adv. Mater. **25**(20), 2826–2830 (2013).
[14] Y. Wang, G. Tsiminis, A. L. Kanibolotsky, P. J. Skabara, I. D. W. Samuel, and G. A. Turnbull, Opt. Express **21**(12), 14362–14367 (2013).
[15] Z. Gong, E. Gu, S. Jin, D. Massoubre, B. Guilhabert, H. Zhang, M. Dawson, V. Poher, G. Kennedy, P. French, and M. Neil, J. Phys. D: Appl. Phys. **41**, 094002 (2008).
[16] H. X. Zhang, D. Massoubre, J. McKendry, Z. Gong, B. Guilhabert, C. Griffin, E. Gu, P. Jessop, J. M. Girkin, and M. D. Dawson, Opt. Expr. **16**(13), 9918–9926 (2008).
[17] M. J. Weber and M. Bass, IEEE J. Quant. Electron. **QE5**(4), 175–188 (1969).
[18] I. Samuel and G. Turnbull, Chem. Rev. **107**, 1272–1295 (2007).
[19] M. Lehnhardt, T. Riedl, U. Scherf, T. Rabe, and W. Kowalsky, Organic Electronics **12**, 1346–1351 (2011).
[20] A. Monkman, C. Rothe, S. King, and F. Dias, Adv. Polym. Sci. **212**, 187–225 (2008).
[21] G. Wegmann, B. Schweitzer, D. Hertel, H. Giessen, M. Oestreich, U. Scherf, K. Müllen, and R. Mahrt, Chem. Phys. Lett. **312**, 376–384 (1999).
[22] R. Bornemann, U. Lemmer, and E. Thiel, Opt. Lett. **31**(11), 1669–1671 (2006).
[23] R. Bornemann, E. Thiel, and P. H. Bolívar, Opt. Express **19**(27), 26382–26393 (2011).
[24] K. Yamashita, K. Hase, H. Yanagi, and K. Oe, Jpn. J. Appl. Phys. **46**(28), L688–L690 (2007).
[25] T. Rabe, K. Gerlach, T. Riedl, H. H. Johannes, W. Kowalsky, J. Niederhofer, W. Gries, J. Wang, T. Weimann, P. Hinze, F. Galbrecht, and U. Scherf, Appl. Phys. Lett. **89**, 081115 (2006).
[26] Z. Gong, S. Jin, Y. Chen, J. McKendry, D. Massoubre, I. M. Watson, E. Gu, and M. D. Dawson, J. Appl. Phys. **107**, 013103 (2010).
[27] J. Herrnsdorf, Organic Lasers and Nano-Patterned Organic Films for Hybrid Integration, PhD thesis, University of Strathclyde, Glasgow, UK, 2012, and references therein.
[28] F. Hu, K. Y. Qian, and Y. Luo, Appl. Opt. **44**(14), 2768–2771 (2005).
[29] E. Matioli and C. Weisbuch, J. Appl. Phys. **109**, 073114 (2011).
[30] J. J. D. McKendry, B. R. Rae, Z. Gong, K. R. Muir, B. Guilhabert, D. Massoubre, E. Gu, D. Renshaw, M. D. Dawson, and R. K. Henderson, IEEE Photon. Technol. Lett. **21**(12), 811–813 (2009).
[31] H. Y. Ryu, and J. I. Shim, Opt. Express **19**(4), 2886–2894 (2011).
[32] A. E. Chernyakov, K. A. Bulashevich, S. Y. Karpov, and A. L. Zakgeim, Phys. Status Solidi A **210**(3), 466–469 (2013).
[33] X. Guo, Y. L. Li, and E. F. Schubert, Appl. Phys. Lett. **79**(13), 1936–1938 (2001).
[34] G. Kranzelbinder, E. Toussaere, J. Zyss, T. Kavc, G. Langer, and W. Kern, Appl. Phys. Lett. **82**(14), 2203–2205 (2003).
[35] A. Rose, Z. Zhu, C. F. Madigan, T. M. Swager, and V. Bulović, Nature **434**, 876–879 (2005).
[36] C. Karnutsch, C. Gärtner, V. Haug, U. Lemmer, T. Farrell, B. S. Nehls, U. Scherf, J. Wang, T. Weimann, G. Heliotis, C. Pflumm, J. C. deMello, and D. D. C. Bradley, Appl. Phys. Lett. **89**, 201108 (2006).
[37] C. Karnutsch, C. Pflumm, G. Heliotis, J. C. deMello, D. D. C. Bradley, J. Wang, T. Weimann, V. Haug, C. Gärtner, and U. Lemmer, Appl. Phys. Lett. **90**, 131104 (2007).
[38] B. K. Yap, R. Xia, M. Campoy-Quiles, P. N. Stavrinou, and D. D. C. Bradley, Nat. Mater. **7**, 376–380 (2008).

[39] R. Xia, W. Y. Lai, P. A. Levermore, W. Huang, and D. D. C. Bradley, Adv. Funct. Mat. **19**, 2844–2850 (2009).
[40] R. Gupta, M. Stevenson, and A. J. Heeger, J. Appl. Phys. **92**(9), 4874–4877 (2002).
[41] A. Dodabalapur, M. Berggren, R. E. Slusher, Z. Bao, A. Timko, P. Schiortino, E. Laskowski, H. E. Katz, and O. Nalamasu, IEEE J. Sel. Top. Quantum. Electron. **4**(1), 67–74 (1998).
[42] W. Y. Lai, R. Xia, Q. Y. He, P. A. Levermore, W. Huang, and D. D. C. Bradley, Adv. Mater. **21**, 355–360 (2009).
[43] Z. Xu, Q. Liao, Q. Shi, H. Zhang, J. Yao, and H. Fu, Adv. Mater. **24**, OP216–OP220 (2012).
[44] V. G. Kozlov, V. Bulović, P. E. Burrows, and S. R. Forrest, Nature **389**, 362–364 (1997).
[45] V. G. Kozlov, V. Bulovic, P. E. Burrows, M. Baldo, V. B. Khalfin, G. Parthasarathy, and S. R. Forrest, J. Appl. Phys. **84**(8), 4096–4108 (1998).
[46] M. Berggren, A. Dodabalapur, R. E. Slusher, and Z. Bao, Nature **389**, 466–469 (1997).
[47] M. R. Krames, O. B. Shchekin, R. Mueller-Mach, G. O. Mueller, L. Zhou, G. Harbers, and M. G. Craford, J. Display Technol. **3**(2), 160–175 (2007).
[48] Y. Chen, J. Herrnsdorf, B. Guilhabert, A. L. Kanibolotsky, A. R. Mackintosh, Y. Wang, R. A. Pethrick, E. Gu, G. A. Turnbull, P. J. Skabara, I. D. Samuel, N. Laurand, and M. D. Dawson, Org. Electron. **12**, 62–69 (2011).
[49] C. Ge, M. Lu, X. Jian, Y. Tan, and B. T. Cunningham, Opt. Express **18**(12), 12980–12991 (2010).
[50] E. M. Calzado, J. M. Villalvilla, P. G. Boj, J. A. Quintana, V. Navarro-Fuster, A. Retolaza, and M. A. Díaz-García, Appl. Phys. Lett. **101**, 223303 (2012).
[51] J. Herrnsdorf, B. Guilhabert, Y. Chen, A. L. Kanibolotsky, A. R. Mackintosh, R. A. Pethrick, P. J. Skabara, E. Gu, N. Laurand, and M. D. Dawson, Opt. Express **18**(25), 25535–25545 (2010).